Presented at the International Technical Meeting, ION GNSS 2008, September 16-19, Savannah, Georgia

Impact of Near-Field Effects on the GNSS Position Solution

Florian Dilßner
Logica, Darmstadt, Germany

Günter Seeber
Institut für Erdmessung, Universität Hannover, Germany

Gerhard Wübbena, Martin Schmitz
Geo++®, Gesellschaft für satellitengestützte geodätische und navigatorische Technologien mbH
Garbsen, Germany

BIOGRAPHY

Dr. Florian Dilßner received his degrees in Geodesy from the Universität Hannover. He has been working in the field of GNSS as a research assistant at the Universität Hannover since 2003 focusing on absolute GNSS antenna field calibration and GNSS station calibration. He is now working for Logica Germany as a technical consultant at the Navigation Support Office of the European Space Operations Centre (ESA-ESOC).

Dr. Günter Seeber has been Professor at the Institut für Erdmessung, Universität Hannover since 1973, where he teaches satellite geodesy, geodetic astronomy and marine geodesy. He has specialized in satellite positioning techniques since 1969 and has published several scientific papers and books in the field of satellite and marine geodesy.

Dr. Gerhard Wübbena and Dr. Martin Schmitz received their degrees in geodesy from the Universität Hannover. Dr. Wübbena has worked in the field of GNSS since 1983. In 1990 he founded the company Geo++®, which develops satellite navigation and positioning software and systems. Among these are the post-processing system GEONAP and the real time system GNSMART. Dr. Schmitz has been working in the field of GNSS since 1991. He worked as a research fellow at the Universität Hannover and for the industry. Both authors are currently employed at Geo++®. They are concerned with research and development in satellite positioning. Current projects focus on highly precise RTK phase positioning (GNSMART), absolute GNSS antenna field calibration, GNSS station calibration and real time attitude systems.

ABSTRACT

The objective of this paper is to give an insight into the near-field effect with respect to the coordinate domain. With the aid of Hannover´s Automated Absolute Antenna Field Calibration Technique developed by the Institut für Erdmessung (Universität Hannover) and Geo++® we demonstrate that mechanical structures mounted underneath the antennas (e.g. tribrachs, tripod heads, etc.) can cause significant changes in the phase center offset and variations (PCV) described by the common spherical harmonic model. For the GPS carrier signals L1 and L2 these changes (DPCV) are in the order of several millimeters. Long-term static GPS simulations on a local and global scale prove that during the adjustment process the often quoted "averaging effect due to extended observation periods" does not actually apply to this DPCV signal. It is instead a bias that falsifies the coordinate estimation. Analysis based on the ionospheric-free linear combination L0 and the estimation of tropospheric zenith delay parameters indicate systematic height errors with a magnitude of 1-2 cm for mid-latitude locations. Independent comparisons between the height difference provided by GPS and the height difference measured with an optical precise leveling instrument clearly verify the impact of the near-field effect. Since GPS satellite geometry degrades with increasing station latitude, the bias can reach up to 4-5 cm in polar regions. Thus, we draw the conclusion that for the purpose of precise height determination an antenna calibration accounting for the near-field is imperative. This is true even if "multipath-resistant" geodetic antennas are used that are provided with extended ground planes and additional choke-ring-elements.

INTRODUCTION

GNSS carrier phase multipath in conjunction with signal diffraction still degrades the accuracy especially of high precision static and kinematic positioning. The wide range of proposed methods for multipath estimation and mitigation developed during the last two decades clearly underline the relevance of this issue. Although much effort has been invested in refining antenna designs and in-receiver processing algorithms, multipath signals still seriously affect the GNSS observables. In static applications with highest accuracy requirements (e.g. establishment and densification of geodetic reference frames), it is commonly assumed that multipath effects completely average out for extended observation periods. However, the hypothesis of zero mean multipath seems to be valid only in the case of short periodic multipath signals caused by distant objects located in the far-field region of the antenna. In fact, long periodic errors due to reflections from the closest vicinity of the antenna are non-zero mean distributed and therefore introduce an unmodeled bias in the estimated parameters. Moreover, reflecting surfaces located in the so-called near-field region of the antenna can change the overall electromagnetic properties due to induced currents caused by antenna coupling effects. We will refer to the resulting phase error as "near-field effect".

GEOMETRIC MULTIPATH MODEL

Multipath propagation means that the signal reaches the antenna on two or more paths. Generally, the antenna will capture the direct line-of-sight signal superimposed by one or more of its reflections from objects in the vicinity and from the ground. In a simple geometric multipath model with one reflecting surface (Figure 1), the carrier phase error for an isotropic antenna is described as

$$\Psi = \tan^{-1} \frac{\alpha \cdot \sin \Delta\Phi}{1 + \alpha \cdot \cos \Delta\Phi}, \qquad (1)$$

where α denotes the attenuation of the voltage amplitude, with $\alpha = 0$ in the case of no reflection and $\alpha = 1$ in the case of an identical signal strength of the reflected and direct signal (e.g. Georgiadou and Kleusberg 1988). The amplitude ψ_{max} of the multipath error signal can be described as a function of the inverted sine of α. For small values ($\alpha << 1$) ψ_{max} nearly depends linearly on α.

The phase shift $\Delta\Phi$ between direct and reflected signal is given by

$$\Delta\Phi = \frac{2\pi}{\lambda} \cdot \Delta d, \qquad (2)$$

with λ representing the carrier wavelength and Δd the excess of path of the reflected signal with respect to the direct one. Assuming a single, infinitely large, horizontal reflector plane one obtains geometrically

$$\Delta d = 2h \cdot \sin \varepsilon, \qquad (3)$$

where h is the perpendicular distance of the antenna phase center from the reflector plane and ε the elevation angle of the incident signals (cf. Figure 1).

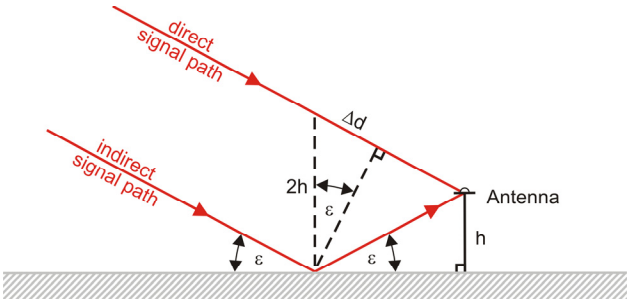

Figure 1: Geometric multipath model.

The multipath error for the "ionosphere-free" signal L0 - the linear combination of the GPS L1 and L2 phase observables commonly used for coordinate estimation in regional and global networks - can be derived as follows:

$$\Psi_{L0} = 2.5457 \cdot \Psi_{L1} - 1.5457 \cdot \Psi_{L2}, \qquad (4)$$

whereas the multipath error ψ_{L1} belongs to the wavelength of L1 (λ_1 = 190.3 mm) and ψ_{L2} to the wavelength of L2 (λ_2 = 244.2 mm).

The frequency of the multipath error ψ varies according to

$$f_\Psi = \frac{2h}{\lambda} \cdot \cos \varepsilon \cdot \frac{d\varepsilon}{dt}. \qquad (5)$$

It can be noticed that the frequency f_ψ is proportional to the reflector distance h, the cosine of the satellite elevation ε and the rate of change $d\varepsilon/dt$ of the elevation. Hence, slow ascending or descending satellites tend to have significantly longer multipath signal periods compared to satellites showing a higher rate of change of the elevation. If the phase center is located h_1 = 2.0 m above the reflector surface, the period lengths of the multipath signals are in the magnitude of several minutes. In this case, the excess signal path Δd for satellites above $\varepsilon > 15°$ is between 1 m < Δd < 3 m. If the phase center is just h_2 = 0.1 m away from the reflector surface, Δd is below 0.2 m and the period length of the multipath signal may reach a few hours (Figure 2).

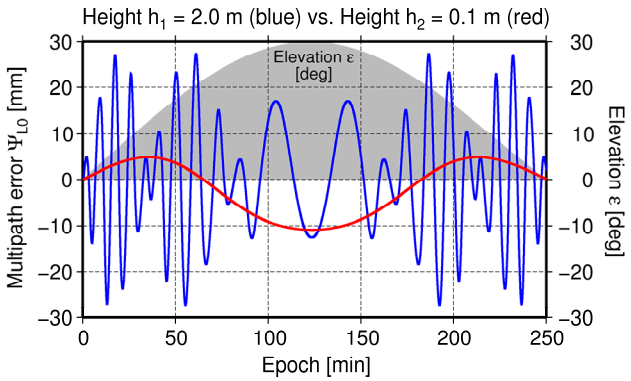

Figure 2: Simulated multipath signal ψ_{L0} for a horizontal reflector surface using two different heights and a fixed damping factor α of 0.2.

Unfortunately, state-of-the art receiver based mitigation techniques against multipath mainly focus on C/A and L2C code-observables and are still ineffective in the case of a short excess signal path Δd. If the direct signal and the indirect signal arrive just within approximately 100 ns or 30 m, the receiver processing algorithms cannot distinguish between the desired direct signal and the reflected signal. In the case of carrier phase multipath, the boundary where mitigation is not possible anymore is probably reached at $\Delta d_{min} \approx 1$ m (Weill 1997). Moreover, long-term static GPS analysis simulations based on the geometric multipath model given by (1) have indicated that only distant reflector's multipath with high frequency can be reduced effectively by averaging over sufficient periods of time and that a bias Δz in the estimates of the vertical coordinate can generally be expected if the distance h between the antenna phase center and the reflector plane is short (Dilßner 2007). This contradicts the popular notion that carrier phase multipath can always be eliminated simply through averaging.

NEAR-FIELD AND FAR-FIELD

The geometric multipath model described in the previous section appears to provide a useful approximation for the multipath error (Elósegui et al. 1995). However, it does not account for the complex electromagnetic field characteristics arising in the immediate vicinity of the antenna. Following Balanis (2005), the radiating field of an antenna can be subdivided into three regions: reactive near-field, radiating near-field and far-field (Figure 3).

The boundaries separating these regions are related to the wavelength λ of the signal and the maximum overall dimension D of the antenna. The transitions between the regions are gradual. Various definitions have been developed to identify the boundaries of the field regions (Capps 2001). For GNSS antennas operating in the ultra high frequency range, the far-field (Fraunhofer) region is commonly taken to begin at a distance of

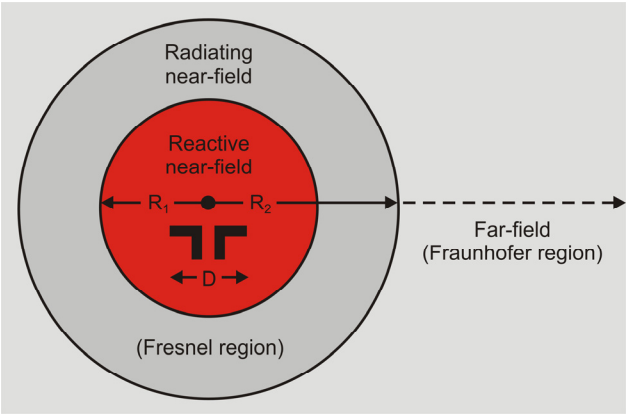

Figure 3: Field regions of an antenna (Balanis 2005).

$$R_2 = \frac{2D^2}{\lambda}. \qquad (6)$$

In the far-field region, geometrical ray optics provides an appropriate method in describing the wave propagation. The wave front is considered planar and rays are parallel. The shape of the radiation pattern is independent of the distance r and the electromagnetic properties of the antenna itself are not affected by objects entering the far-field region.

The distances where the simplified planar, parallel ray approximation breaks down are known as the near-field region. The near-field region is commonly divided into two more subregions (Balanis 2005). The transition from the reactive near-field to the far-field is the so-called radiating near-field (Fresnel) region. The inner boundary of this region is taken to be the radial distance

$$R_1 = 0.62 \cdot \sqrt{\frac{D^3}{\lambda}} \qquad (7)$$

and the outer boundary is at R_2. Within the radiating near-field the radiation pattern depends on the distance r from the antenna. If the maximum antenna dimension D is very small compared to λ the region may not exist. The field region closest to the antenna is called the reactive near-field. It is taken to exist in a range of $0 < r < R_1$.

The near-field is of particular relevance since it forms the far-field transmission or reception pattern of an antenna. It can be visualized as a resonant reservoir that stores energy in the air surrounding the antenna. If lossy material with higher permittivity than air ($e_r = 1$) enters the near-field region, energy is getting absorbed and thus is no longer available for the antenna. In the worst case, the presence of conductive structures changes the effective size of the antenna reception element and thereby becomes part of the antenna.

GNSS receiving antennas are frequently mounted on massive concrete pillars or steel pylons. Since the permittivity of concrete and metal is much higher than air and the structures are well located in the near-field region, changes in the electromagnetic properties of the antennas are to be expected. But not only the permanently installed GNSS reference stations may suffer from near-field effects. For many high precision surveying campaigns and monitoring tasks, different adaptation for the antenna mounts are designed, e.g. to incorporate a prism for simultaneous point monitoring by conventional total stations and GNSS.

AUTOMATED ABSOLUTE FIELD CALIBRATION

In many analyses, Hannover's Automated Absolute Field Calibration has proven to be one of the most accurate techniques for the determination of absolute antenna phase center offsets and phase center variations (PCV). The fundamental concept of this calibration method is based on the rigorous separation between phase center characteristics and site dependent multipath effects (Menge et al. 1998, Wübbena et al. 2000). Other than for relative calibration approaches, the results are completely independent from environmental multipath as well as from the phase center characteristics of the used reference antenna. By means of a precisely calibrated and fast moving robot, the test antenna is tilted and rotated. These quick changing antenna orientations are essential for the calibration. Since time differences between consecutive epochs amount to just a few seconds, the environmental multipath error is highly correlated and can be well described as a stochastic process within a Kalman-Filter. To avoid any potential multipath not eliminated by mathematical modeling, a high elevation mask of 18° is used, which is dynamically adopted for tilted orientations. Further error components such as ionospheric, tropospheric and orbit biases cancel out using a very close-by reference station. Due to this observation procedure, it is possible to obtain eventually a clear PCV signal free of residual systematic effects. Depending on the particular satellite constellation, one calibration data set consists of a dense and homogeneous coverage of around 6000 to 8000 measurement epochs without any geographical station dependencies like the northern hole. The model describes the complete antenna hemisphere down to zero degree elevation by means of a spherical harmonic expansion of degree n_{max} and order $m_{max} \le n_{max}$:

$$PCV(\alpha,\varepsilon) = \sum_{n=0}^{n_{max}} \sum_{m=0}^{m_{max}} (a_{nm} \cos m\alpha + b_{nm} \sin m\alpha) \cdot P_{nm}(\sin \varepsilon) \quad (8)$$

The resulting phase center variations are depending on azimuth α and elevation angle ε. Measurements below the antenna horizon (-5°) are operationally incorporated to strengthen the model at zero degree elevation. For each carrier frequency, the spherical harmonic coefficients a_{nm} and b_{nm} are estimated within the Kalman-Filter process. In order to define the radius of the sphere the condition PCV for zenith equals null is used.

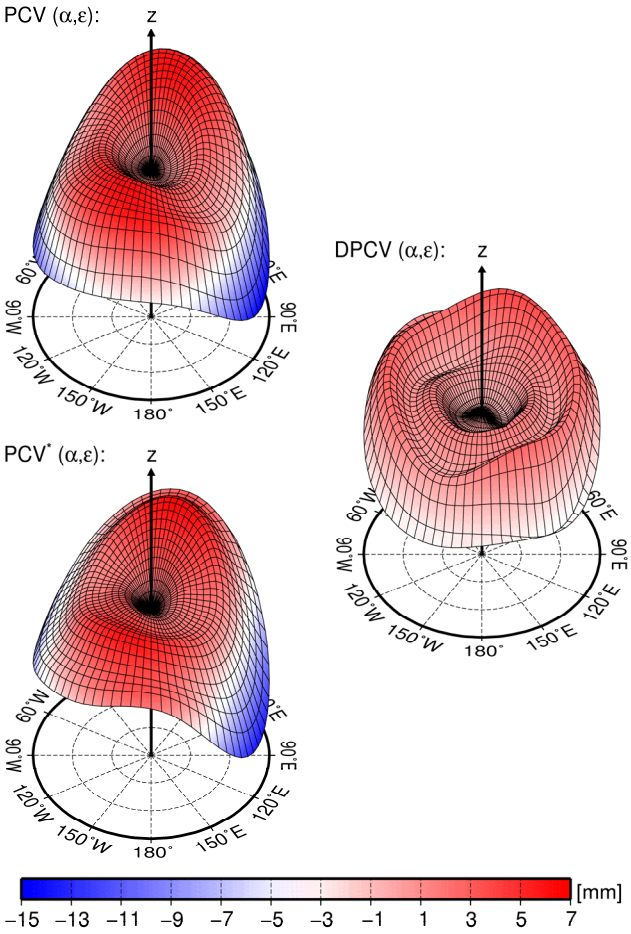

Figure 4: PCV from stand-alone calibration (top), PCV* from near-field calibration (bottom) and DPCV (middle). The data are based on the calibration of an ASH700700B rover antenna with and without metal plate (cf. Figure 5).

In order to verify the appearance and to reveal the magnitude of antenna near-field effects, the Automated Absolute Field Calibration has also proven to be a well suitable technique (Wübbena et al. 2003, Schmitz et al. 2004, Dilßner et al. 2006, Lesparre 2006). For this type of investigation, the antenna has to be mounted on the robot together with a representative model of the real antenna environment (e.g. the actual mount). During the calibration process, the presence of this near-by surface model will now change the overall electromagnetic properties of the antenna. Moreover, long-period multipath signals can be expected. Because the geometric relationship between antenna and environment mock-up is constant, reflections coming from the same direction with respect to the antenna coordinate system, induce the same multipath signal. Therefore, the antenna near-field effect is not eliminated by the calibration observation procedure.

Instead, an additional phase pattern (DPCV) caused by the near-field effect superimposes the PCV signal. Subtracting the measured PCV* pattern from the PCV pattern obtained in a standard antenna calibration, provides the DPCV pattern representing the near-field influence (Figure 4).

ANTENNA SETUPS

In the framework of a first antenna calibration series, the near-field effects on two rover antennas and on two geodetic antennas equipped with extended ground planes have been investigated. First of all, the antennas were calibrated regularly in stand-alone mode. For the near-field calibrations, each test candidate was mounted once over a circular metal plate (diameter = 27.0 cm) and once over a circular tripod head (diameter = 16.5 cm). Both constructions were connected to the particular test antenna by means of a geodetic tribrach. The three setting screws of the tribrach were not changed during the whole test series in order to ensure a comparable distance (≈ 6 cm) between antenna and metal surface. Moreover, the antenna test candidates were installed on a custom-built model which has been designed by the State Survey of Saxony-Anhalt (LVermGeo) in the context of the modernization and renewal of the national height reference system. The adaptation was developed to directly fix a leveling rod near the GNSS antenna allowing parallel measurements of ellipsoidal heights by GNSS and heights by precision leveling (Figure 5).

Figure 5: Antenna test candidate TRM39105.00 mounted over the metal plate (left), the tripod head (middle) and the special adaption for fixing a leveling rod (right).

Within a second test series, we investigated two more geodetic antenna models, one equipped with a choke-ring ground plane and another one using Stealth™ ground plane technology (Krantz et al. 2001). Both antennas were provided by the Bavarian State Survey (LVG) together with a special metallic tube (Figure 6).

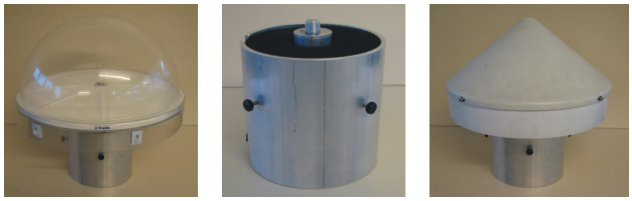

Figure 6: Antenna test candidates TRM41249.00_TZGD (left) and LEIAT503_LEIC (right) mounted on a metal cylinder (middle).

The tube has been filled with foamed material. According to the LVG, the basic idea behind the tube is to install it permanently at certain GNSS network sites in order to shield the station antennas from near-field effects. However, before the installation, the near-field influence of the tube itself should be quantified.

All antenna setups are summarized in Table 1. The mechanical structures have been mounted directly underneath the antennas. The largest diameter of the smallest test antenna is D = 165 mm. The equivalent wavelength for the ionosphere-free linear combination L0 is λ = 107 mm. According to the far-field condition (6), the radius of the sphere defining the boundary between near-field and far-field is 51 cm. For the tested geodetic antennas equipped with the conventional extended ground plane of a diameter of 482 mm the boundary is located even at 434 cm. Therefore, we can conclude that the mechanical structures are well located within the near-field region of each antenna test candidate.

	metal plate	tripod head	leveling adaption	metal cylinder
ASH700700B	P1	T1	A1	-
TRM39105.00	P2	T2	A2	-
TRM14532.00+GP	P3	-	A3	-
TRM33429.20+GP	P4	T4	A4	-
TRM41249.00_TZGD	-	-	-	C5
LEIAT503_LEIC	-	-	-	C6
LEIAT503_LEIC*	-	-	-	C7

Table 1: Setup IDs for the antenna near-field calibrations (* different GPS receiver used).

QUANTIFICATION OF NEAR-FIELD EFFECTS

In this section the PCV differences (DPCV) between near-field setups and regular stand-alone calibrations are presented. The PCV of each antenna calibration have been modeled with a spherical harmonic expansion of degree n_{max} = 8 and order m_{max} = 5. However, in lack of space, we only refer to the elevation-dependent parts here which have been computed based on a spherical harmonic expansion of degree n_{max} = 8 and order m_{max} = 0. The elevation-dependent DPCV found for L1 and L2 are in the order of ±4 mm (Figure 8 - Figure 9). For some regions near the horizon the effects in azimuthal direction are even larger. Since the L1 and L2 contributions are commonly of different sign, the DPCV of the ionosphere-free linear combination L0 are getting amplified by a factor of three (Figure 10). In the case of setup P1, a maximum value of +13 mm can be noticed. It should be noted that the DPCV found for the setups P3 and P4 are quite similar due to comparable antenna design and dimension. The same applies for the DPCV of A3 and A4.

The smallest DPCV have been found for the setups with the metallic tube (C5, C6). Although the good performance of the metallic tube is an indication to a reduction of near-field effects with a somehow controlled mounting, we believe that it may change the intentional design of the antenna itself. Without analyzing other antenna properties like the gain pattern, a user may significantly alter an antenna in other characteristics.

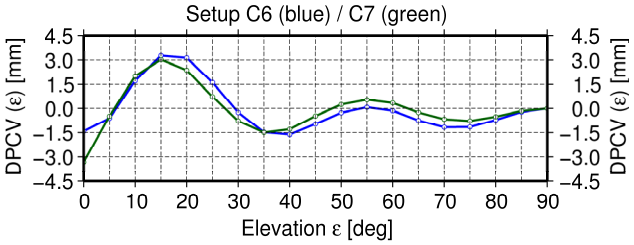

Figure 7: Repeatability for L0.

In order to verify the repeatability of the DPCV and to identify possible receiver related tracking dependencies, we have done one more stand-alone calibration and one more near-field calibration for the antenna setup C6, but now with a GPS receiver from a different manufacturer. This new setup has been denoted as C7. Comparing the elevation-dependent DPCV belonging to setups C6 and C7, it can be noticed that the repeatability of the DPCV for L0 is generally better than 1 mm (Figure 7).

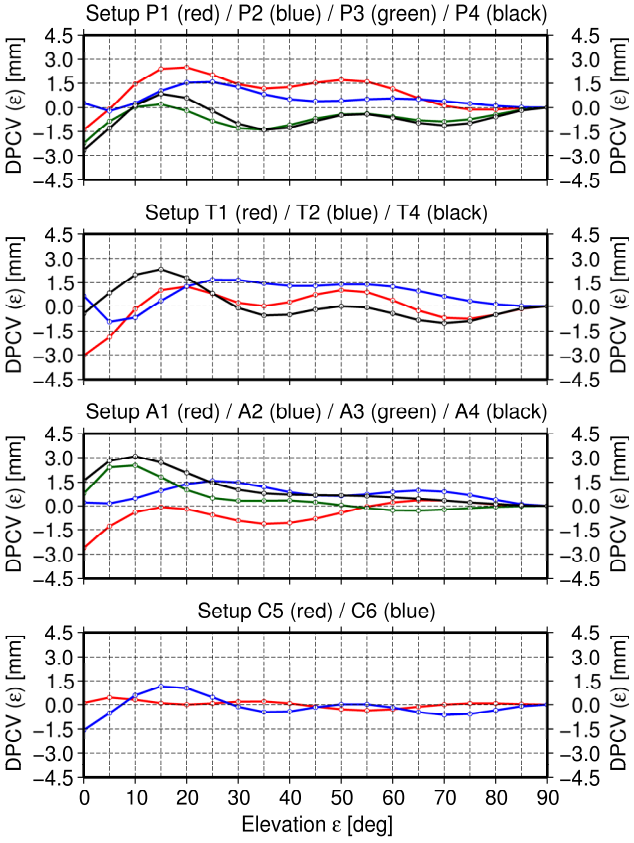

Figure 8: Elevation-dependent near-field effects for L1.

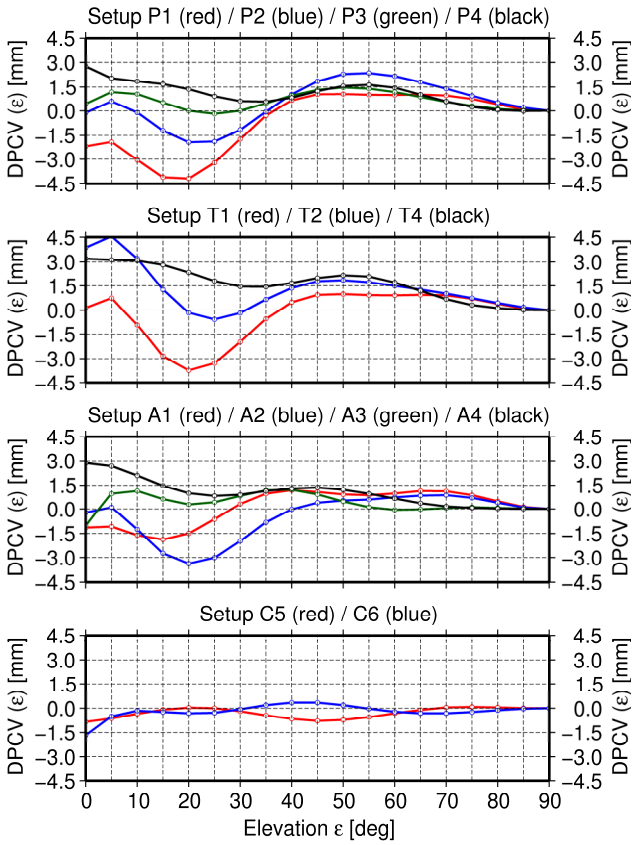

Figure 9: Elevation-dependent near-field effects for L2.

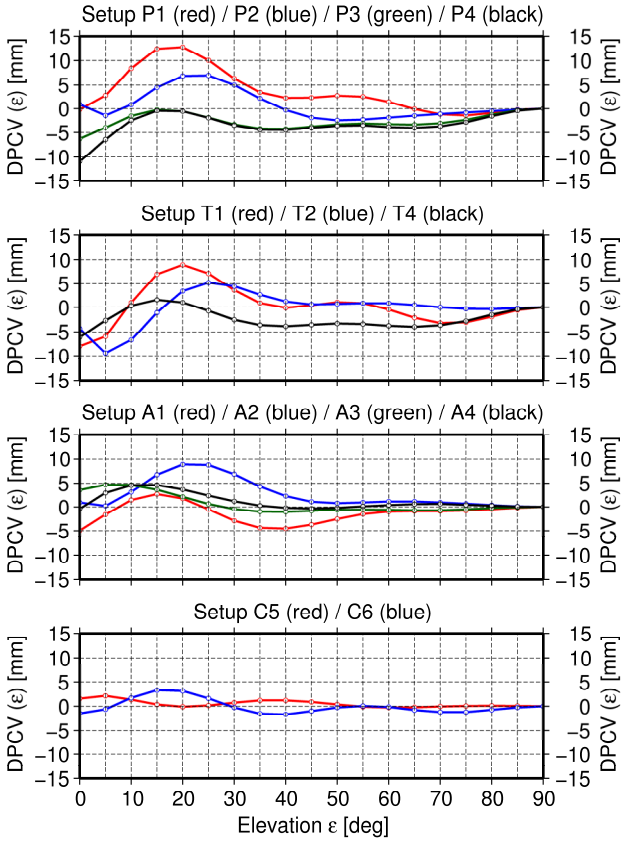

Figure 10: Elevation-dependent near-field effects for L0.

SIMULATION STRATEGY

A simple GPS analysis tool based on (between-receiver) observation single-differences has been developed in order to answer the question how the systematic near-field pattern obtained from the antenna calibration propagates into the GPS position solution. In this context, we have computed three types of solution simulating different scenarios: a short baseline (L1+L2), a medium baseline (L0) and a long baseline (L0+T). We consider the baseline length to be short when the station distance is less than 1 km and to be long when the distance exceeds 50 km. The parameters belonging to each simulation scenario are summarized below (Table 2).

Solution ID	Baseline length	Parameters
L1+L2	0 … 1 km	Δx, Δy, Δz, Δc, Δf
L0	1 … 50 km	Δx, Δy, Δz, Δc
L0+T	50 km …	Δx, Δy, Δz, Δc, Δt

Table 2: Parameters of the simulation scenarios

The DPCV are treated as pseudo-observations. In order to underline that we are not estimating absolute parameters but only relative biases we precede each parameter variable with a "Δ". We solve for three coordinate components Δx, Δy, Δz expressed in a left-handed local geodetic system and one receiver clock parameter Δc per epoch expressed also in length units.

In the case of the solution type L1+L2, we simulate a dual-frequency analysis based on the original L1 and L2 carrier phase observables. Hence, we have to consider additionally an inter-frequency bias parameter Δf absorbing common signal delays between L1 and L2. For the other scenarios, this parameter is irrelevant since we make use of the ionosphere-free linear combination L0. In the case of the L0+T solution, we also take a relative tropospheric (wet) zenith delay parameter Δt into account. The results obtained for L0+T are thereby also valid for absolute precise point positioning (PPP). For the projection of the zenith path delay into slant direction, we make use of a simple elevation dependent cosecant model. It should be mentioned in this context that additional mapping functions for troposphere estimation have been implemented into our analysis software. However, it turned out that the choice of the mapping function generally does not affect the coordinate bias caused by the near-field (Dilßner 2007).

The parameter estimation is done over an observation span of 24 hours based on the satellite distribution for a given site located at the University of Hannover (Figure 11). In a further step, we extend the computations to a global grid. Since the DPCV near-field pattern as well as the partial derivatives of the GNSS observation equation with respect to the unknowns is a function of the satellite direction, it can be expected that the parameter biases vary with the latitude of the observer's site, because the GPS satellite distribution is a function of the site's latitude (Santerre 1991). Even changes in the space segment will have an effect when considering GNSS (re-) processing campaigns with data from different years (see below). The DPCV signal will mostly be absorbed in the receiver clock, station height and troposphere parameters, since the partial derivatives of these parameters show strong elevation dependence similar to the DPCV pattern (Figure 12).

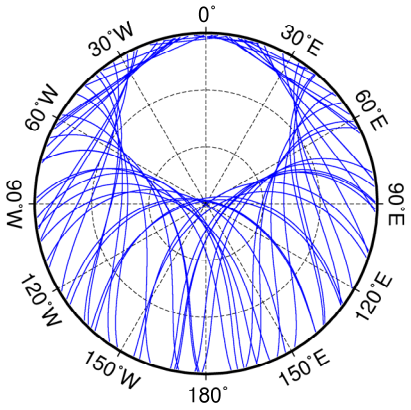

Figure 11: GPS satellite sky view at the University of Hannover (φ = 52.38° N, λ = 9.70° E) for a 24-hour period, 13 January 2006. The center of the plot represents the zenith (ε = 90°), the outer circle the horizon (ε = 0°).

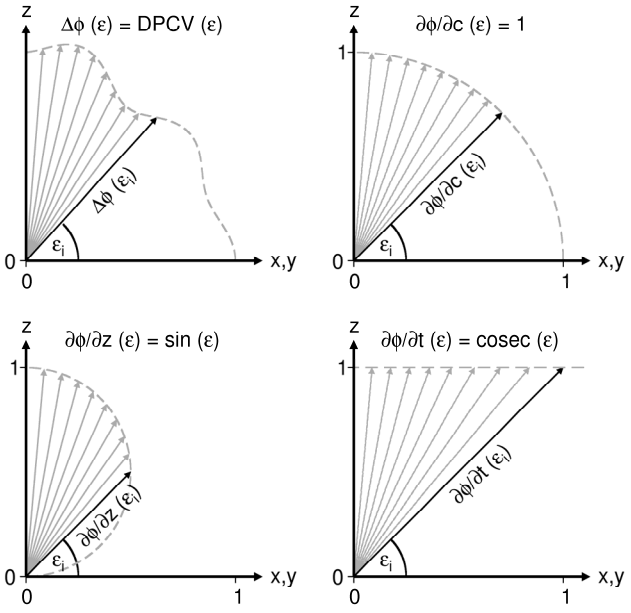

Figure 12: Elevation dependence of the DPCV (left-top) and the partial derivatives of receiver clock parameter Δc (right-top), station height parameter Δz (left-bottom) and tropospheric zenith delay parameter Δt (right-bottom).

Our simulation is based on several generalizations, hence, only the single station dependent impact of the near-field effect is obtained. It is assumed that ionospheric refraction effects are reduced effectively due to the shortness of the baseline (in the case of solution L1+L2) and due to the use of the ionosphere-free linear combination L0. We also assume that the carrier phase ambiguities have already been fixed to their integer values in a previous step. They are treated as deterministic constants and are not part of the parameter estimation process anymore. In real life applications with multiple stations we still have superimposed effects from differences in antenna types, Earth's curvature causing different local verticals and satellites appearing under different elevations, up to orbit errors, to name a few.

The choice of the right observation weighting strategy in connection with the elevation cut-off setting has always been a controversial issue in GNSS analysis. Since low elevation data are commonly much more susceptible to multipath and tropospheric refraction, users generally tend to apply the elevation-dependent variance model

$$\sigma_n^2(\varepsilon) = \frac{\sigma_0^2}{\sin^2(\varepsilon)}, \qquad (9)$$

whereas σ_0 represents the measurement noise for the zenith. The downside of this approach is that the information inherent in low-elevation observations is not fully exploited. Therefore, some people prefer equal observation weighting in combination with individual elevation cut-off settings. In view of our near-field analysis, we have tested both weighting schemes including different elevation cut-off settings. The standard-deviation σ_0 has been set to 1 mm.

The parameter estimation is done within a discrete Kalman-Filter algorithm, since the stochastic properties of the parameters ("state variables") can simply be described as time-dependent stochastic processes and the relatively small dimension of the state vector will not lead to much longer computation time compared to the performance of a least-square Gauss-Markov estimator. The static character of the station coordinates can be expressed as a non-dynamic random-constant process. Epoch-wise (kinematic) coordinate estimation can easily be simulated using a white noise process. The receiver clock error Δc is also treated as white noise with a sufficient high process variance whereas the inter-frequency bias Δf is modeled as an integrated white noise ("random-walk") process using a variance of 2 mm. The temporal correlations in the tropospheric zenith path delay are characterized by a first-order Gauss-Markov process using a variance of 2 cm and a correlation length of 2 hours.

While investigating the stochastic settings of the Kalman-Filter it turned out that the process variance for the clock parameter Δc and the inter-frequency parameter Δf have hardly any effect on our coordinate estimates. Besides, Δc and Δf can simply be removed from the observation equation through (receiver-satellite) double-differencing without any information loss (Lindlohr and Wells 1985). Consequently, when running our simulation algorithm in double-difference processing mode, we found exactly the same coordinate biases as in the single-differencing mode. In order to ensure that the functional modeling and stochastic tuning of the Kalman-Filter algorithm actually yields to proper results we processed some of the DPCV data with the scientific GNSS software package GEONAP (Wübbena 1989). The coordinate biases computed with our simulation tool and with GEONAP are fully consistent within a few sub-millimeters.

SIMULATION RESULTS

Table 3 and Table 4 show the obtained vertical bias Δz. It can be noticed that Δz strongly depends on the analysis strategy and the antenna model. For the solutions based on L1+L2, the bias is rather small. In the case of the setups involving the geodetic antennas, Δz is in the order of only 1-2 mm, but in the case of the L0 and L0+T estimates we found biases of up to 15 mm for the geodetic antennas and of up to 23 mm for the rover antennas. It is interesting to see that in several cases the bias gets amplified by a factor of 10 due to troposphere estimation whereas in other cases the troposphere parameter absorbs the near-field signal yielding to a significant reduction of the bias Δz. Comparing the different analysis strategies, it seems that excluding near-field signals from the processing by setting up the elevation cut-off angle or down weighting them by using an elevation-dependent function does not always reduce Δz. For the sake of completeness, it should be mentioned that the effects on the estimates of the horizontal coordinates were only in the order of 1-3 mm.

	L1+L2			L0			L0+T		
ID	0°	8°	15°	0°	8°	15°	0°	8°	15°
P1	-3	-2	-2	5	14	18	15	19	2
P2	-2	-2	-2	4	8	12	8	16	5
P3	0	1	0	0	2	2	3	0	-11
P4	1	2	1	-2	3	3	4	2	-10
T1	-1	-2	-2	-2	9	16	11	23	6
T2	0	-1	-1	-7	-2	7	-2	21	16
T4	2	3	2	1	5	5	6	3	-9
A1	-1	-1	-1	1	4	4	4	-1	-19
A2	-1	-2	-3	2	7	11	7	15	6
A3	2	2	1	7	7	5	6	0	-7
A4	2	2	2	4	6	5	6	2	-6
C5	0	0	0	1	0	0	0	0	4
C6	0	1	1	2	4	5	5	2	-9
C7	0	1	1	1	4	3	4	0	-9

Table 3: Estimated bias Δz [mm] applying unit weighting.

ID	L1+L2			L0			L0+T		
	0°	8°	15°	0°	8°	15°	0°	8°	15°
P1	-2	-2	-2	14	14	15	15	10	-1
P2	-2	-2	-3	9	9	10	9	6	-5
P3	0	1	0	0	0	-1	-2	-7	-15
P4	1	2	1	1	1	0	0	-5	-13
T1	-1	-1	-2	11	12	14	16	14	3
T2	0	-1	-1	5	6	8	12	17	11
T4	2	3	2	3	3	2	1	-5	-13
A1	-1	-1	-1	0	0	-1	-3	-10	-20
A2	-1	-2	-3	8	8	9	10	8	-2
A3	2	2	1	3	3	2	0	-4	-8
A4	2	2	2	3	3	3	1	-2	-8
C5	0	0	0	1	1	1	1	2	4
C6	0	1	1	2	2	2	1	-3	-9
C7	0	0	1	2	2	1	0	-3	-7

Table 4: Estimated bias Δz [mm] applying elevation-dependent sinus weighting.

INFLUENCE OF SATELLITE GEOMETRY

We can proceed from the assumption that the near-field effect does not change over time, as long as the closest vicinity of the antenna remains unchanged. Thus, since the GPS ground track repeats approximately after every sidereal day (23 h 56 min 4 s) (Seeber et al. 1997), we can expect that the coordinate bias caused by the near-field influence will repeat for 24 h data sets from day-to-day. It should be noted that GPS orbits tend to drift off from their nominal ground tracks and maneuvers are required by the GPS Control Segment to reposition the satellites (Figure 13). However, the variations in the ascending node are generally in the order of ±2°, which is comparatively small with respect to the resolution of our spherical harmonic function describing the DPCV model. In addition variations due to changes in the space segment (number of available satellites) must be anticipated. Consequently, the computed DPCV signals nearly repeat from day-to-day. Variations in time are to some extend caused by differences in the space segment.

In order to verify the aforementioned assumption, we processed stepwise the broadcast ephemeris of all visible satellites for each day between 1st January 1994 and 31st December 2005. The site has the coordinates of Hannover (cf. Figure 11). As further input data, we have used the near-field DPCV patterns obtained from the calibrations of the four antenna setups P1, P2, P3 and P4. The data has been weighted equally and the elevation cut-off angle has been set to 8°. The daily L0+T estimates of the vertical bias Δz are shown in Figure 14. As one can see from the figure, the bias actually remains constant within ±1.5 mm which means that the effect cannot be reduced through averaging over several days, weeks or even years. Moreover, we detect timely variations of similar order for all setups, but no conspicuous (e.g. annual) signal periods in the time-series. Hence, as long as the near-field pattern does not change over time, we can conclude that neglecting the effect does not cause any additional signals yielding to misinterpretations in the analysis of long-term coordinate time series. However, a small time dependency exists, which may degrade the accuracy.

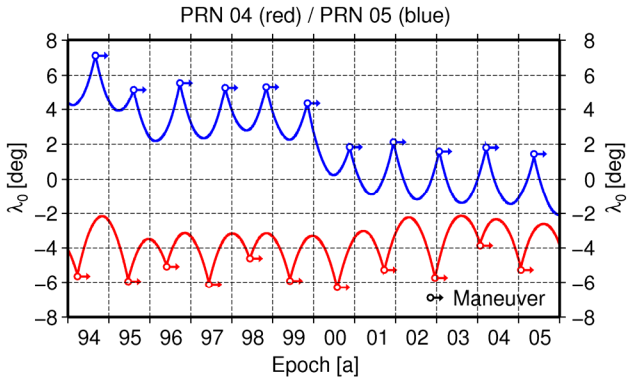

Figure 13: Variations in the longitude λ_0 of the ascending nodes of two GPS-satellites over a time span of 12 years.

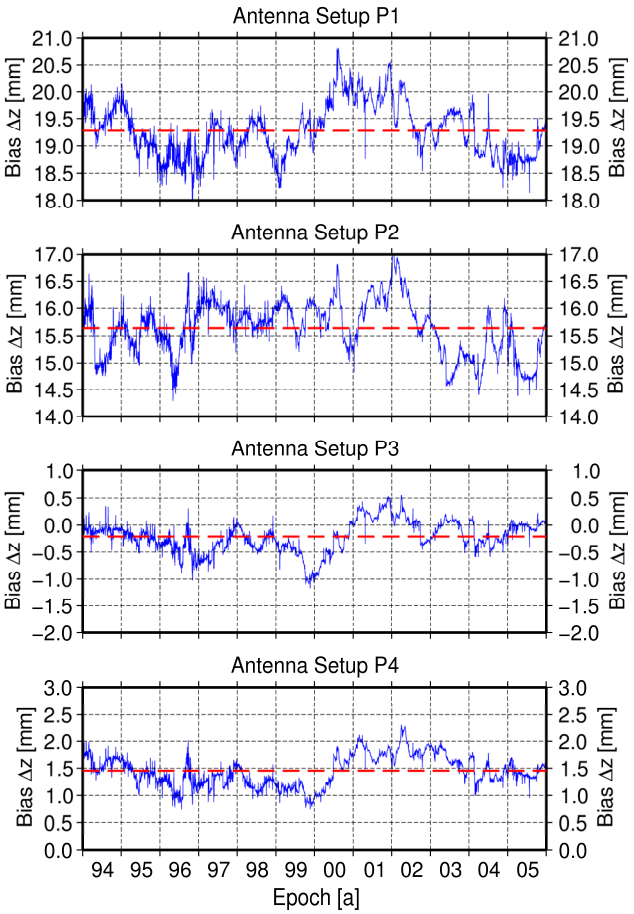

Figure 14: Daily L0+T estimates of the vertical bias Δz for a site located at the University of Hannover (φ = 52.38° N, λ = 9.70° E) over a time span of 12 years.

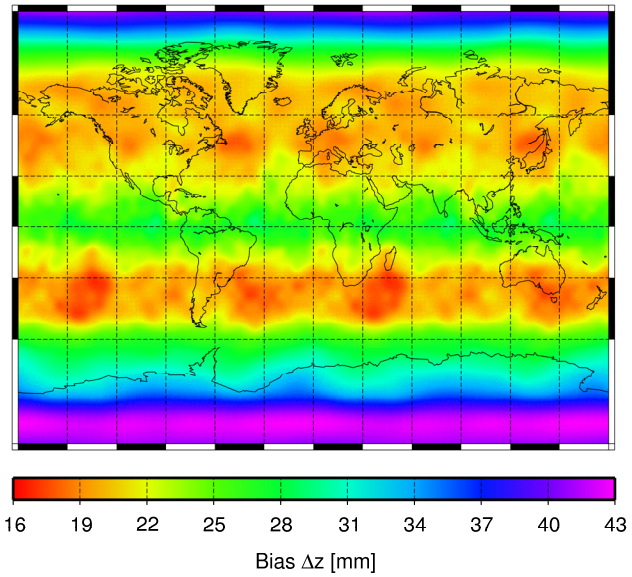

Figure 15: Global variation of L0+T estimates of the vertical bias Δz based on the DPCV of antenna setup P1.

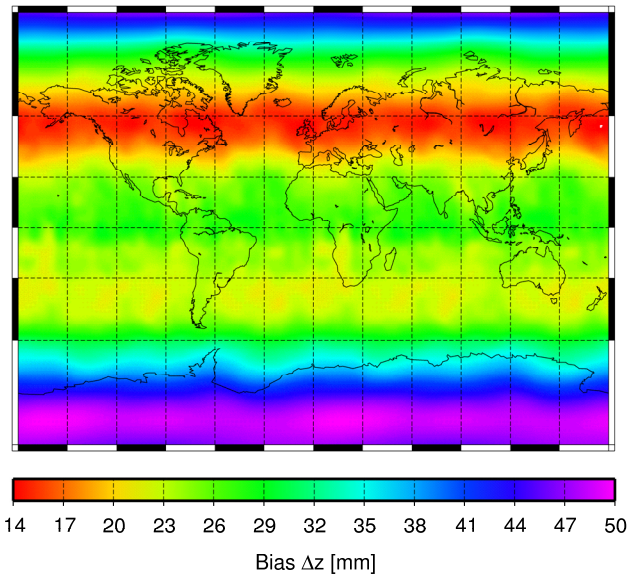

Figure 16: Global variation of L0+T estimates of the vertical bias Δz based on the DPCV of antenna setup P2.

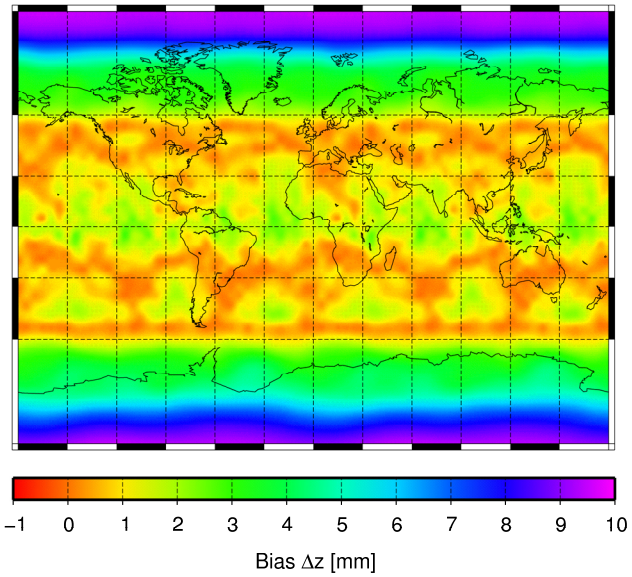

Figure 17: Global variation of L0+T estimates of the vertical bias Δz based on the DPCV of antenna setup P3.

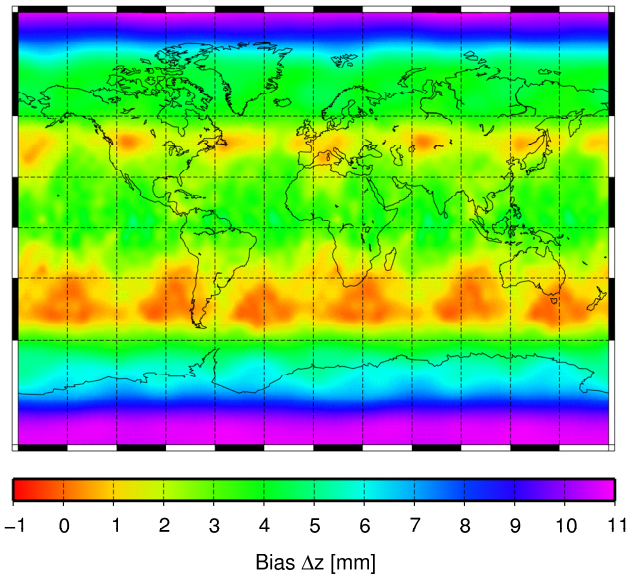

Figure 18: Global variation of L0+T estimates of the vertical bias Δz based on the DPCV of antenna setup P4.

Since the DPCV patterns describing the near-field effect as well as several elements of the design matrix – or to be more precisely, the partial derivatives of the observations with respect to the station coordinates and the troposphere parameter – are functions of the satellite azimuth and elevation, we can expect that the resulting parameter biases will also depend on the particular geographic position of the observer's site. In order to analyze this dependency in more detail, we have shifted the latitude φ and longitude λ of our local topocentric coordinate system stepwise and re-computed the vertical bias. The parameter estimation is simulated again over an observation span of 24 hours, but now with respect to the GPS satellite constellation for an observer's site located at the latitude φ_i and the longitude λ_j. The DPCV data have been weighted equally and the elevation cut-off angle has been set to 8°. The L0+T estimates of Δz_{ij} (φ_i, λ_j) based on the DPCV patterns of the four different antenna setups P1, P2, P3 and P4 are shown above (Figure 15 - Figure 18). Due to the degradation of the satellite geometry with increasing station latitude, the bias obviously can triple in polar regions. In the case of the larger near-field patterns found for the antenna setups P1 and P2, it may even reach up to 4-5 cm (cf. Figure 15 - Figure 16).

In terms of rapid static or real-time kinematic (RTK) applications, we can expect additional time dependent variations in the estimated coordinate biases, since the observation span is usually only several minutes or even only one epoch long and the satellite geometry is therefore not fully exploited. The examples shown below demonstrate the behaviour of the vertical bias Δz for epoch-wise L0 coordinate estimation (Figure 19).

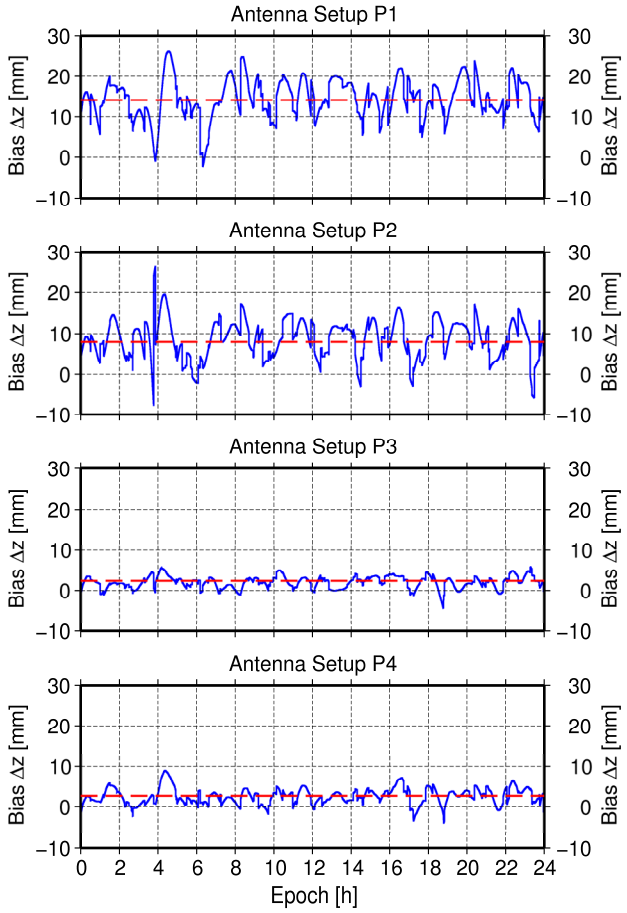

Figure 19: Time dependent variations of epoch-wise L0 estimates of the vertical bias Δz for a site located at the University of Hannover (φ = 52.38° N, λ = 9.70° E).

SHORT BASELINE MEASUREMENTS

In order to give a further proof of the existence of near-field effects and their dependency with respect to the analysis strategy and the antenna model we carried out GPS field measurements on a very short baseline located on the roof of the Geodetic Institute of the University of Hannover. The antennas were installed on concrete pillars which are separated by approximately 8 m. Due to the shortness of the baseline we can avoid all distance-dependent error components. Three 24 hour data sets were collected at 1 Hz sampling rate.

We have used a pair of geodetic choke-ring antennas (Figure 20) for the first session (B1) and a pair of rover antennas without extended ground planes (Figure 21) for two more sessions (B2, B3). The antennas were mounted on metallic geodetic tribrachs. In order to induce additional near-field effects, a metal plate having a diameter of 60 cm was installed on top of one of the pillars. The perpendicular distance between the metal plate and the bottom side of the antenna was approximately 10 cm.

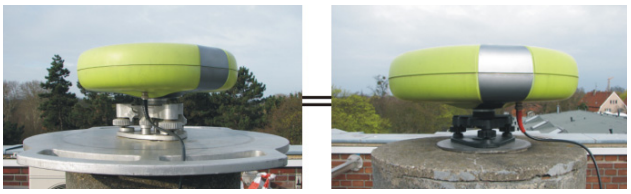

Figure 20: Pillars with choke-ring antennas (setup B1).

Figure 21: Pillars with rover antennas (setup B2, B3).

The analysis was performed using the scientific GNSS software package GEONAP (Wübbena 1989). We did not introduce individual PCV corrections into the analysis, but verified that the individual phase center characteristics of the respective antennas are nearly identical. The baseline components were estimated based on the L1+L2, L0 and L0+T solutions applying equal observation weighting in combination with different elevation cut-off settings. The table below (Table 5) shows the height difference provided by GPS minus the height difference measured with an optical precise leveling instrument. In the case of the setups B2 and B3, a bias of up 11 mm can be noticed. The setup B3 shows actually the repeatability of the experiment B2 after one week. The results also indicate, that the choke-ring antenna used in the setup B1 is less affected compared to the rover antenna. For permanently operating reference stations it is therefore an advantage to use a choke-ring antenna.

	L1+L2			L0			L0+T		
ID	0°	8°	15°	0°	8°	15°	0°	8°	15°
B1	1	1	1	2	2	0	3	3	5
B2	0	1	0	8	7	5	4	4	7
B3	1	2	0	11	10	4	5	4	11

Table 5: Comparisons between the height difference provided by GPS and the height difference measured with an optical precise leveling instrument in [mm].

For the actual application of near-field corrections obtained from the Automated Absolute Antenna Field Calibration we refer to Wübbena et al. (2006) and Lesparre (2006). In an operational RTK network it has been demonstrated that height biases due to near-field effects could be completely removed.

CONCLUSIONS

We draw the conclusion that for the purpose of precise height determination an antenna calibration accounting for the near-field is imperative. However, concerning size and weight, our robot has limited capabilities to handle antenna constructions. Consequently, remaining near-field interactions as well as multipath effects coming from surfaces located in the far-field have to be captured by alternative approaches of actual station calibrations.

One such method has been developed using basically the robot to realize a "multipath-free" reference station (Böder 2001). Due to a continuous but (pseudo-) random motion of the robot's antenna in all directions from a center position, the systematic multipath effects on that particular station are removed. Since precise absolute PCV are known and distance-dependent errors cancel out, the multipath of a second station is accessible. It is an ideal reference system to determine the complete absolute multipath effects of one particular station.

Applying this in-situ calibration technique to the baseline measurements described in the previous section has yielded a reduction of the vertical bias of about 90 percent (Dilßner 2007). The temporal validity of the correction parameters is determined by the satellites´ orbit properties and largely depend on how accurately multipath errors and receiver clock errors can be separated within the modeling process. The combined use of GPS, GLONASS and GALILEO promises a significant increase in information and additional possibilities for in-situ station calibration.

SUMMARY

Using Hannover´s Automated Absolute Antenna Field Calibration Technique, we determined near-field patterns for several antenna mounts and antenna models. The systematic near-field errors were mapped into the positioning domain. Based on the processing of 12 years of GPS broadcast ephemeris we demonstrated that the resulting bias Δz in the vertical coordinate component is actually a height bias for 24 h data sets. Moreover, it was shown that Δz strongly depends on the site's latitude and the GNSS analysis strategy. The dependency on satellite constellation and status of space segment has been demonstrated, which relevance increases for reduced observation time and is most important for RTK applications. While using the original L1 and L2 observables for data processing, the impact is small, but the height bias Δz can amount to a significant magnitude, if atmospheric delays have to be taken into account. Using the ionosphere-free linear combination L0 in combination with the estimation of a tropospheric zenith delay parameter can amplify Δz by a factor of ten. Excluding the near-field signals from the GNSS data processing by setting up the elevation cut-off angle or down weighting the effect using an elevation-dependent function is not always an appropriate way to reduce the effect. The need of effective methods for station calibration is underlined by the conducted near-field analysis.

ACKNOWLEDGMENTS

The work described in this paper was supported in part by the State Survey and Geospatial Basic Information Lower Saxony (LGN) and the Ernst Simon Foundation. We acknowledge the support provided by the State Survey of Saxony-Anhalt (LVermGeo) and the Bavarian State Survey (LVG).

REFERENCES

Balanis, C.A. (2005): Antenna Theory. Third Edition, John Wiley & Sons, New York.

Böder, V., F. Menge, G. Seeber, G. Wübbena, M. Schmitz (2001): How to Deal with Station Dependent Errors - New Developments of the Absolute Calibration of PCV and Phase-Multipath with a Precise Robot. In: Proceedings of the 14th International Technical Meeting of the Satellite Division of the Institute of Navigation ION GPS 2001, September 11-14, Salt Lake City, Utah, USA.

Capps, C. (2001): Near-field or far-field? EDN Magazine, August 16, 95-102.

Dilßner, F., G. Seeber, M. Schmitz, G. Wübbena, G. Toso, D. Maeusli (2006): Characterisation of GOCE SSTI Antennas. ZfV, Zeitschrift für Vermessungswesen, 131, Heft 2, 61-71.

Dilßner, F. (2007): Zum Einfluss des Antennenumfeldes auf die hochpräzise GNSS-Positionsbestimmung. Ph.D. thesis, Wissenschaftliche Arbeiten des Fachrichtung Geodäsie und Geoinformatik der Leibniz Universität Hannover, Nr. 271.

Elosegui, P., Davis, J.L., Jaldehag, R.K., Johansson, J.M., Niell, A.E., Shapiro, I.I. (1995): Geodesy using the Global Positioning System: The effects of signal scattering on estimates of site position. Journal of Geophysical Research, 100, 9921-9934.

Georgiadou, Y., A. Kleusberg (1988): On carrier signal multipath effects in relative GPS positioning. Manuscripta Geodaetica 13, 172-179.

Krantz, E., S. Riley, P. Large (2001): The Design and Performance of the Zephyr Geodetic Antenna. In: Proceedings of the 14th International Technical

Meeting of the Satellite Division of the Institute of Navigation ION GPS 2001, September 11-14, Salt Lake City, Utah, USA.

Lesparre, J. (2006): The impact of the antenna mounting on the phase centre variation. EUREF-Symposium, June 14-17, Riga, Latvia.

Lindlohr, W., D.E. Wells (1985): GPS design using undifferenced carrier bat phase observations. Manuscripta Geodaetica 10, 255-295.

Menge, F., G. Seeber, C. Völksen, G. Wübbena, M. Schmitz (1998): Results of Absolute Field Calibration of GPS Antenna PCV, In: Proceedings of the 11th International Technical Meeting of the Satellite Division of the Institute of Navigation ION GPS-98, September 15-18, Nashville, Tennessee, USA.

Santerre, R. (1991): Impact of GPS satellite sky distribution. Manuscripta Geodaetica 16, 28-53.

Schmitz, M., G. Wübbena, G. Boettcher (2004): Near Field Effects of a Car Roof on TPSHIPER_PLUS Phase Variations. Geo++® White Paper, Garbsen.

Seeber, G., F. Menge, C. Völksen, G. Wübbena, M. Schmitz (1997). Precise GPS Positioning Improvements by Antenna and Site Dependent Effects. In: IAG Symposium, No. 115, Springer Verlag.

Stutzman, W.L., G.A. Thiele (1998): Antenna Theory and Design. Second Edition, John Wiley & Sons, New York.

Weill, L. R. (1997): Conquering Multipath: The GPS Accuracy Battle. GPS World, Vol. 8, No. 4, 59-66.

Wübbena, G. (1989): The GPS Adjustment Software Package -GEONAP- Concepts and Models. In: Proceedings of the Fifth International Symposium on Satellite Positioning, Las Cruces, New Mexico.

Wübbena, G., M. Schmitz, F. Menge, V. Böder, G. Seeber (2000): Automated Absolute Field Calibration of GPS Antennas in Real-Time. In: Proceedings of the 13th International Technical Meeting of the Satellite Division of the Institute of Navigation ION GPS 2000, September 19-22, Salt Lake City, Utah, USA.

Wübbena, G., M. Schmitz, G. Boettcher (2003): Zum Einfluss des Antennennahfeldes. 5. GPS-Antennen-Workshop 2003 im Rahmen des 5. SPOS-Symposiums. 3. November 2003, Frankfurt am Main.

Wübbena, G., M. Schmitz, G. Boettcher (2006): Near-field Effects on GNSS Sites: Analysis using Absolute Robot Calibrations and Procedures to Determine Corrections. In: Proceedings of the IGS Workshop 2006 Perspectives and Visions for 2010 and Beyond, May 8-12, ESOC, Darmstadt, Germany.